Multi-walled carbon nanotube physicochemical properties predict pulmonary inflammation and genotoxicity

Poulsen, Sarah S.; Jackson, Petra; Kling, Kirsten; Knudsen, Kristina B.; Skaug, Vidar; Kyjovska, Zdenka O.; Thomsen, Birthe L.; Clausen, Per Axel; Atluri, Rambabu; Berthing, Trine; Bengtson, Stefan; Wolff, Henrik; Jensen, Keld A.; Wallin, Håkan; Vogel, Ulla Birgitte

Published in:
Nanotoxicology

Link to article, DOI:
10.1080/17435390.2016.1202351

Publication date:
2016

Document Version
Publisher's PDF, also known as Version of record

Nanotoxicology

ISSN: 1743-5390 (Print) 1743-5404 (Online) Journal homepage: http://www.tandfonline.com/loi/inan20

Multi-walled carbon nanotube physicochemical properties predict pulmonary inflammation and genotoxicity

Sarah S. Poulsen, Petra Jackson, Kirsten Kling, Kristina B. Knudsen, Vidar Skaug, Zdenka O. Kyjovska, Birthe L. Thomsen, Per Axel Clausen, Rambabu Atluri, Trine Berthing, Stefan Bengtson, Henrik Wolff, Keld A. Jensen, Håkan Wallin & Ulla Vogel

To cite this article: Sarah S. Poulsen, Petra Jackson, Kirsten Kling, Kristina B. Knudsen, Vidar Skaug, Zdenka O. Kyjovska, Birthe L. Thomsen, Per Axel Clausen, Rambabu Atluri, Trine Berthing, Stefan Bengtson, Henrik Wolff, Keld A. Jensen, Håkan Wallin & Ulla Vogel (2016) Multi-walled carbon nanotube physicochemical properties predict pulmonary inflammation and genotoxicity, Nanotoxicology, 10:9, 1263-1275, DOI: 10.1080/17435390.2016.1202351

To link to this article: http://dx.doi.org/10.1080/17435390.2016.1202351

http://informahealthcare.com/nan
ISSN: 1743-5390 (print), 1743-5404 (electronic)

Nanotoxicology

Nanotoxicology, 2016; 10(9): 1263–1275
 DOI: 10.1080/17435390.2016.1202351

Taylor & Francis
Taylor & Francis Group

ORIGINAL ARTICLE

Multi-walled carbon nanotube physicochemical properties predict pulmonary inflammation and genotoxicity

Sarah S. Poulsen[1]*, Petra Jackson[1]*, Kirsten Kling[1], Kristina B. Knudsen[1], Vidar Skaug[2], Zdenka O. Kyjovska[1], Birthe L. Thomsen[1], Per Axel Clausen[1], Rambabu Atluri[1], Trine Berthing[1], Stefan Bengtson[1], Henrik Wolff[3], Keld A. Jensen[1], Håkan Wallin[1,4], and Ulla Vogel[1,5]

[1]*National Research Centre for the Working Environment, Copenhagen Ø, Denmark,* [2]*National Institute of Occupational Health, Oslo, Norway,* [3]*Finnish Institute of Occupational Health, Helsinki, Finland,* [4]*Institute of Public Health, Copenhagen University, Copenhagen K, Denmark, and* [5]*Department of Micro- and Nanotechnology, Technical University of Denmark, Kgs. Lyngby, Denmark*

Abstract

Lung deposition of multi-walled carbon nanotubes (MWCNT) induces pulmonary toxicity. Commercial MWCNT vary greatly in physicochemical properties and consequently in biological effects. To identify determinants of MWCNT-induced toxicity, we analyzed the effects of pulmonary exposure to 10 commercial MWCNT (supplied in three groups of different dimensions, with one pristine and two/three surface modified in each group). We characterized morphology, chemical composition, surface area and functionalization levels. MWCNT were deposited in lungs of female C57BL/6J mice by intratracheal instillation of 0, 6, 18 or 54 μg/mouse. Pulmonary inflammation (neutrophil influx in bronchoalveolar lavage (BAL)) and genotoxicity were determined on day 1, 28 or 92. Histopathology of the lungs was performed on day 28 and 92. All MWCNT induced similar histological changes. Lymphocytic aggregates were detected for all MWCNT on day 28 and 92. Using adjusted, multiple regression analyses, inflammation and genotoxicity were related to dose, time and physicochemical properties. The specific surface area (BET) was identified as a positive predictor of pulmonary inflammation on all post-exposure days. In addition, length significantly predicted pulmonary inflammation, whereas surface oxidation (–OH and –COOH) was predictor of lowered inflammation on day 28. BET surface area, and therefore diameter, significantly predicted genotoxicity in BAL fluid cells and lung tissue such that lower BET surface area or correspondingly larger diameter was associated with increased genotoxicity. This study provides information on possible toxicity-driving physicochemical properties of MWCNT. The results may contribute to safe-by-design manufacturing of MWCNT, thereby minimizing adverse effects.

Keywords

BET surface area, CNT-length, CNT-diameter, functionalization, lymphocytic aggregates

History

Received 3 December 2015
Revised 29 April 2016
Accepted 2 May 2016
Published online 7 July 2016

Introduction

Carbon nanotubes (CNT) constitute a class, rather than a singular nanomaterial. Commercially available CNT vary greatly in length, thickness, aspect-ratio, curvedness, chemical and chiral-purity, and homogeneity. Many also contain a substantial fraction of impurities that are residues from catalytic agents or manufacturing processing. Relatively few studies (Jackson et al., 2015; Poland et al., 2008; Poulsen et al., 2015a,b; Rittinghausen et al., 2014) have attempted to correlate the toxicity of CNT with physicochemical properties. Biopersistence, length and rigidity have been proposed to be determinants of CNT toxicity, in analogy with the toxicity of asbestos and other inorganic fibers. However, we recently reported that one short/thin and one longer/thicker MWCNT induced similar pulmonary inflammatory response and similar systemic effects after pulmonary exposure (Poulsen et al., 2015a,b).

CNT are functionalized to achieve altered surface charge, -functionality and -reactivity, stability, and dispensability for specialized applications. Here, we studied the influence of surface oxidation (–OH and –COOH) on pulmonary inflammation and genotoxicity. Studies investigating the effects of these functionalization have reported more, less or the same toxicity as pristine CNT (Hamilton et al., 2013; Liu et al., 2010; Sayes et al., 2006; Ursini et al., 2012). The chemistry required to modify the surface often changes other physicochemical properties. This complicates the identification of surface functionalization-induced effects on toxicity and their significance is still broadly unclear.

Here, we aim at identifying the physicochemical properties that predict inflammation and genotoxicity in lungs of mice after pulmonary deposition of multi-walled carbon nanotubes (MWCNT). To support these findings, pulmonary pathological changes were also assessed. Ten MWCNT were acquired from

*These authors shared first-authorship.

Correspondence: Ulla Vogel, National Research Centre for the Working Environment, Lersø Parkallé 105, DK-2100 Copenhagen Ø, Denmark. Tel: +45 39165200. Fax: +45 39165201. E-mail: ubv@nrcwe.dk

one supplier. Three groups (I–III) were supplied having same length and diameter within each group, and with either none, carboxy- (COOH-), or hydroxyl- (OH-) functionalizations. In addition Group III also included an amino-functionalization. Effects were studied with four doses (0, 6, 18 and 54 μg/mouse), 1, 28 and 92 days after intratracheal instillation, and compared with those of Printex 90 carbon black (162 μg/mouse) and crocidolite asbestos (6 and 18 μg/mouse).

Neutrophil influx in BAL fluid was chosen as the marker of pulmonary inflammation. Neutrophil influx is generally considered a cardinal marker of inflammation (Erdely et al., 2009; Ma-Hock et al., 2009; Morimoto et al., 2012). Previous studies on pulmonary MWCNT-, TiO_2- and carbon black nanoparticle-induced toxicity have shown correlations between neutrophil influx and increases in both pro-inflammatory cytokine and acute phase response mRNA and protein levels (Bourdon et al., 2012b; Bourdon et al., 2012a; Husain et al., 2013; Jackson et al., 2011; Poulsen et al., 2013, 2015b). Neutrophil influx has been shown to correlate with the total surface area of deposited nanoparticles, and with pulmonary acute phase response, using pulmonary *Saa3* mRNA levels as biomarker for pulmonary acute phase response (Duffin et al., 2007; Saber et al., 2013). This links nanomaterial-induced neutrophil influx in BAL fluid with increased risk of cardiovascular disease (Saber et al., 2014).

DNA strand breaks measured by comet assay were chosen as biomarker of genotoxicity. Increased levels of DNA strand breaks in lung tissue have previously been reported after pulmonary exposure to MWCNT (Poulsen et al., 2015b). In addition, some types of MWCNT also induce ROS production: The mechanisms may be the same as reported for carbon black nanoparticles which induce ROS, DNA strand breaks and increased mutation frequency (Jacobsen et al., 2007, 2008). Genotoxicity through DNA strand breaks and oxidative damage can lead to increased risk of cancer development (Cooke et al., 2003; Federico et al., 2007; Valko et al., 2006). One specific type of MWCNT was recently classified as possibly carcinogenic to humans (Group 2B) (Grosse et al., 2014). In addition, a correlation between neutrophil influx in BAL fluid and mutation rates in lung cells from rats exposed to nanomaterials has been reported (Borm & Driscoll, 1996). Similarly, prolonged inflammation has been linked to increased risk of cancer development (reviewed in (Federico et al., 2007)).

Methods

Materials

Ten MWCNT, purchased from Cheap Tubes, Brattleboro, VT, were analyzed, subsampled and named NRCWE-040 – NRCWE-049 (Table 1). The MWCNT were organized in three groups (thin, thick and short, Group I–III, respectively). Each group (I–III) included a pristine, a hydroxyl-, or a carboxy-functionalized type. In addition, Group III included an amino-functionalized type. Carbon black nanoparticles, Printex 90, a gift from Degussa-Hüls (today Evonic), Frankfurt, Germany, and crocidolite asbestos, a gift from Leibniz Research Institute for Environmental Medicine, were included as positive controls (Muhle et al., 1987). Thorough characterization of all the MWCNT has been published previously (Jackson et al., 2015).

Material dispersion

The MWCNT and crocidolite samples were dispersed using the ENPRA dispersion protocol (Jacobsen et al., 2009) at 2.56 mg/ml stock in 0.45 μm MilliQ filtered Nanopure water with 2% (w/v) homologous mouse serum. Printex 90 dispersion was prepared in stock at 3.24 mg/ml in 0.45 μm MilliQ filtered Nanopure water as described previously (Kyjovska et al., 2015). Stocks were

Table 1. Overview of selected physicochemical characteristics of the studied MWCNT and reference materials.

MWCNT group	Code	Type	Source	Length# nm (±SD)	Diameter# nm (±SD)	OH (mmol/g)	BET (m^2/g)	Endotoxin EU/mg	Fe_2O_3* content	CoO* content	NiO* content	MgO* content	MnO* content
GROUP I	NRCWE-040	PRISTINE	Cheaptubes	518.9 (±598)	20.56 (±6.94)	0.35	150	0.01	0.2	0.001	0.56	0.01	0.002
	NRCWE-041	OH	Cheaptubes	1005 (±2948)	26.38 (±11.08)	1.69	152	0.18	0.13	0.001	0.31	0.02	0.001
	NRCWE-042	COOH	Cheaptubes	723.2 (±971.9)	20.5 (±5.32)	4.09	141	–	0.08	0	0.21	0.03	0.001
GROUP II	NRCWE-043	PRISTINE	Cheaptubes	771.3 (±3471)	26.73 (±6.88)	0.18	82	0.26	0.008	0.001	1.2	0.01	–
	NRCWE-044	OH	Cheaptubes	1330 (±2454)	32.55 (±14.4)	0.23	74	0.25	0.004	0.002	1.04	0.02	–
	NRCWE-045	COOH	Cheaptubes	1553 (±2954)	28.07 (±13.85)	0.63	119	0.27	1.17	0.25	1.34	0.02	0.002
GROUP III	NRCWE-046	PRISTINE	Cheaptubes	717.2 (±1214)	17.22 (±5.77)	0.63	223	0.34	0.008	0.25	0.0045	0.22	0.3
	NRCWE-047	OH	Cheaptubes	532.5 (±591.9)	12.96 (±4.44)	0.26	216	0.19	0.007	0.25	0.0043	0.22	0.3
	NRCWE-048	COOH	Cheaptubes	1604 (±5609)	15.08 (±4.69)	0.58	185	0.01	0.007	0.24	0.0037	0.19	0.28
	NRCWE-049	NH_2	Cheaptubes	731.1 (±1473)	13.85 (±6.09)	0.33	199	0.03	0.004	0.25	0.0038	0.19	0.29
Ref. Mat.	Printex 90	–	Evonik	ND	9	ND	182	0.05	0.006	–	0.0003	–	–
	Crocidolite	–	Leibniz IUF	90% < 4500£	90% < 460£	ND	5.24	0.37	7.23$	-$	-$	0.19$	0.03$

Detailed data published in Jackson et al. (2015). *Determined by WDXRF. Chemical composition data were calculated wt% of the oxides of the elements determined. All Fe is calculated as Fe^{3+}. #Determined by computerized image analysis of SEM micrographs. $: Measured in 2% serum; £: Detailed data published by Muhle et al. (1987); –: Not detected; ND: Not determined.

sonicated in 4–6 ml volumes for 16 min using a 400 W Branson Sonifier S-450D (Branson Ultrasonics Corp., Danbury, CT) mounted with a disruptor horn, operated at 10% amplitude and cooled on ice water. Prior to instillation, dilutions of stocks were again sonicated for 2 min.

Material characterization

The morphology of MWCNT dispersed by sonication in vehicle or ethanol was further characterized by semi-automatic scanning electron microcopy (SEM) and size distributions were determined by dynamic light scattering (DLS). See Supplementary files for details.

Animal handling and study design

Female mice C57BL/6J BomTac aged 6–7 weeks (19 ± 1.5 g) were obtained from Taconic Europe (Ejby, Denmark). All mice were dosed by a single intratracheal instillation at 8 weeks of age. MWCNT were instilled one material at a time at doses 0, 6, 18 and 54 μg/mouse, with a total of 33 mice per vehicle control group and 7 mice per dose group for each time point. Printex 90 was instilled at 162 μg/mouse and crocidolite was instilled at 6 and 18ug/mouse ($N = 7$/group). Mice were euthanized 1, 28 and 92 days post-exposure. Additional mice were allocated for histopathological analyses on day 28 (54 μg/mouse) and 92 (all doses): 3 mice per dose group and 9 vehicle mice in total per time point. All procedures complied with the EC Directive 86/609/EEC and Danish law regulating experiments with animals (The Danish Ministry of Justice, Animal Experiments Inspectorate, permission 2006/561-1123). For more details see Supplementary files.

Analyses of toxicity

Pulmonary inflammation was assessed by differential cell count and total protein content in the bronchoalveolar lavage (BAL) fluid. Genotoxicity was evaluated as DNA strand breaks (%TDNA) by the comet assay in BAL cells, lungs and liver. Histopathological changes were assessed in the lung. See Supplementary files for details.

Statistical analysis

The effects of exposure and dose were analyzed by a factorial design for each day separately by the Analysis of Variance (ANOVA) General Linear Model procedure in Minitab v.15 (Minitab Inc., State College, PA). Correlations and multiple regression analyses were performed in SAS version 9.3 (SAS Institute Inc., Cary, NC) (see Supplementary files).

The pairwise associations between physicochemical parameters (BET surface area, Fe, Mn, Ni, Co, Mg, diameter, length and functionalization) were investigated graphically in a Pearson's Correlation analysis. A single MWCNT (NRCWE-045) differed strongly from the others for several physicochemical parameters. All other MWCNT showed a cluster of highly correlated parameters: BET surface area, diameter, Mn, Co and Ni (Table 2). These parameters could therefore not be separated in the present dataset. We chose to use BET surface area (log-transformed) as the proxy variable in the multiple regression analyses. In the Supplementary files, we also present the results using log-transformed diameter, since it was equally biologically relevant for some endpoints.

OH- and COOH-functionalization was determined by the same combustion elemental analysis: Functionalization levels were calculated under the assumption that all oxygen atoms were either OH or COOH, respectively (Jackson et al., 2015). Oxygen content was therefore chosen as OH-functionalization as the regression variable in the further analyses. Statistical significance was determined at the 0.01 level in the multiple regression analyses, since no other correction for mass-significance was performed.

Results

Exposure characterization

Selected physicochemical characteristics, including surface modifications, specific surface area (BET), endotoxin, Fe_2O_3, CoO, NiO, MgO and MnO content (Table 1) have been reported previously (Jackson et al., 2015). Oxygen content of the hydroxylated and carboxylated MWCNT from Group III was less than that of the pristine, indicating no or very little functionalization.

Scanning electron microscopy

SEM examination of MWCNT and reference materials dispersed in instillation dilutions (Supplementary Figures 1–4) indicated that MWCNT were well dispersed, especially at the low dose. Some agglomeration was observed at the high dose. Functionalization did not seem to influence agglomeration or physical appearance of the MWCNT in dispersion.

MWCNT-lengths were determined by computerized image analysis of SEM micrographs (Table 1). The lengths were not different between Groups I–III. All MWCNT were consistently shorter than declared by the supplier, especially for Group I and II. The length distributions of the MWCNT are displayed in Supplementary Figure 5. In all groups, most of MWCNT were less than 1 μm. However, many MWCNT sub-groups included MWCNT with lengths longer than 5 μm. The MWCNT diameters (Table 1) determined by us and declared by the supplier were consistent. Group II MWCNT were thickest.

Table 2. Pearson's Correlations of physicochemical parameters.

	Length	Diameter	BET	Mn	Mg	Ni	Co	Fe	OH
Length	1	0.3245	−0.3235	0.1299	0.0413	0.0351	−0.0242	−0.0501	0.0738
Diameter	0.3245	1	**−0.8758**	**−0.8904**	**−0.8390**	**0.9095**	**−0.8786**	0.4318	0.0272
BET	−0.3235	**−0.8758**	1	**0.9431**	**0.7794**	**−0.8584**	**0.7648**	−0.1349	0.2524
Mn	0.1299	**−0.8904**	**0.9431**	1	**0.9492**	**−0.9803**	**0.9968**	**−0.8854**	−0.6741
Mg	0.0413	**−0.8390**	**0.7794**	**0.9492**	1	**−0.9801**	**0.9881**	−0.6326	−0.022
Ni	0.0351	**0.9095**	**−0.8584**	**−0.9803**	**−0.9801**	1	**−0.9805**	0.5421	0.0190
Co	−0.0242	**−0.8786**	**0.7648**	**0.9968**	**0.9881**	**−0.9805**	1	−0.6471	0.0188
Fe	−0.0501	0.4318	−0.1349	**−0.8854**	−0.6326	0.5421	−0.6471	1	0.5952
OH	0.0738	0.0272	0.2524	−0.6741	−0.022	0.0190	0.0188	0.5952	1

All variables were log-transformed. Pairwise correlated parameters with correlation coefficiencies more than 0.75 or less than −0.75 are highlighted in bold.

Dynamic light scattering analysis of MWCNT in stock dispersions

All MWCNT types were generally well-dispersed in stock and instillation dispersions. The dispersions were stable after sonication, as indicated by the stable size-distribution (Supplementary Table 1).

MWCNT distribution in the lung

Overall, intratracheal instillation of MWCNT resulted in an even distribution across most of the lung-tissue sections, with a predominant distribution in the centrilobular area. MWCNT appeared as more or less densely packed black deposits in the alveolar macrophages and in foreign body granulomas, and with some MWCNT residing freely in the alveoli (Figure 1B–D). Representative images of lung tissue from mice instilled with Group I MWCNT on day 28 and 92 days are presented in Figure 1(G–L). This MWCNT group was chosen as it includes the most functionalized MWCNT (Table 1). MWCNT deposits were found in both lungs but were more numerous in the left lung (Supplementary Table 2). Material-containing macrophages were observed more often in the lungs of mice from the high dose groups, compared to the lower dose groups.

Animal weight

The weight of mice instilled with MWCNT and vehicle controls was determined at instillation and on day 1, 7, 28, 61 and 92. All mice exhibited similar growth, except for a few mice instilled with 6 µg NRCWE-040, which had significantly lower weight after 28 days (data not shown), but not after 92 days.

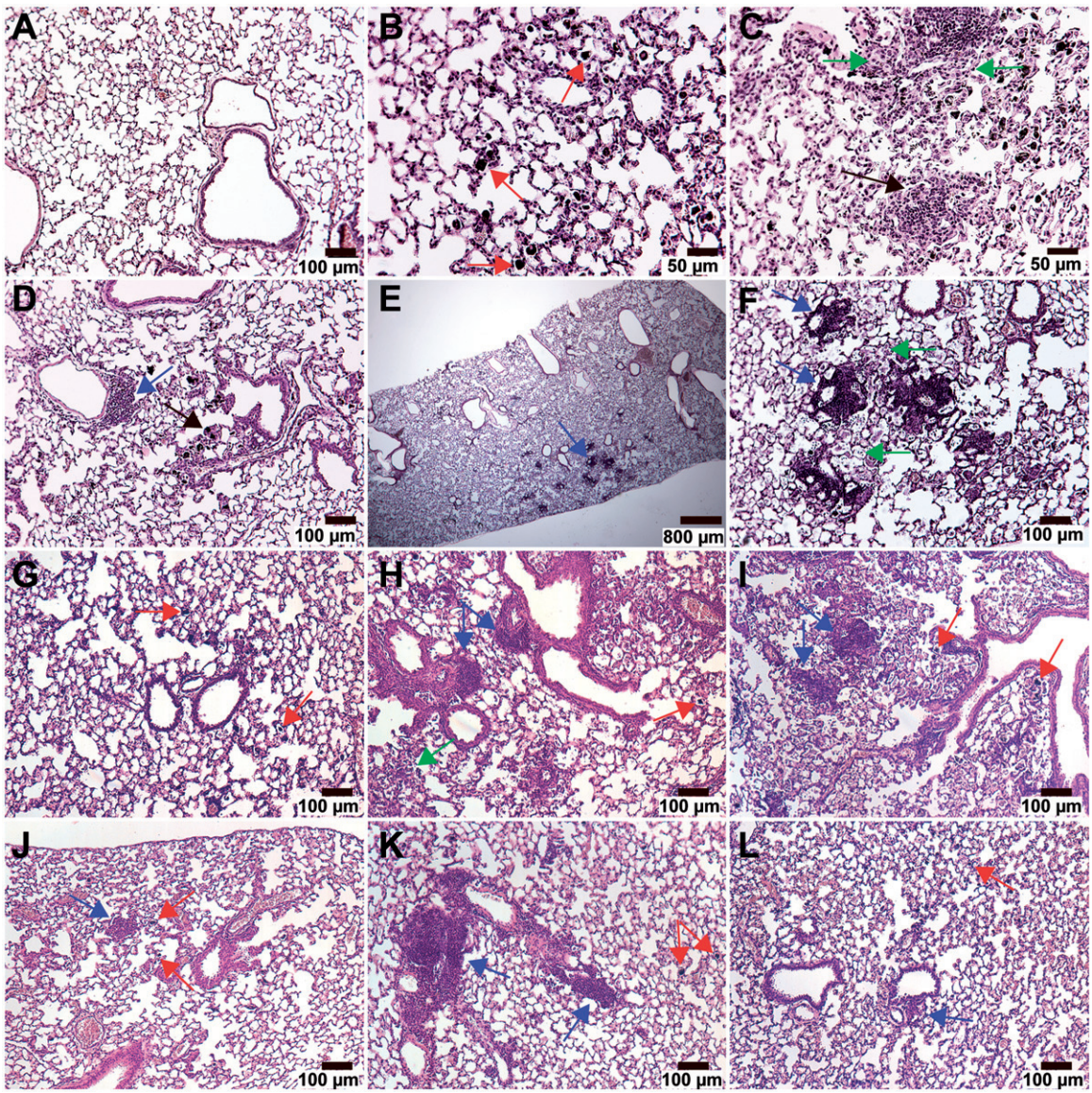

Figure 1. H&E stained histopathological lung sections of mice exposed to 0 or 54 µg MWCNT. (A–F) Representative images of the most predominant histological changes. (G–L) Representative images of Group I MWCNT on day 28 (G–I) and 92 (J–L). Lymphocytic aggregates (Lycy) and foreign material-containing alveolar macrophages where found in all groups of mice exposed to 54 µg MWCNT and are commonly marked with blue and red arrows, respectively, across all images. Objectives are 10× unless otherwise stated. (A) Negative control on day 92. (B) NRCWE-041 on day 92. MWCNT are mainly localized in alveolar macrophages (red arrows). Objective 20×. (C) NRCWE-040 on day 92. Non-dust granuloma (black arrow). Non-collagenous, slight thickening of alveolar ducts and alveolar walls, with hyperplasia of type II cells (green arrows). Objective 20×. (D) NRCWE-040 on day 92. Small CNT-laden (foreign body) granulomas (black arrow). Small perivascular Lycy (blue arrow). (E and F) NRCWE-045 on day 28. Small area of perivascular Lycy (blue arrows). Focal alveolitis (green arrows). For image E the objective was 2×. (G) NRCWE-040 on day 28. (H) NRCWE-041 a on day 28. Slight focal alveolitis, with inflammatory cells and debris in alveoli (green arrow). (I) NRCWE-042 on day 28. (J) NRCWE-040 on day 92. (K) NRCWE-041 on day 92. (L) NRCWE-042 on day 92.

Neutrophil counts in bronchoalveolar lavage fluid

BAL fluid cell composition was determined on day 1, 28 and 92 (Supplementary Table 3). Inflammation as neutrophil influx differed both between the MWCNT Groups (I–III) and the functionalization groups (pristine, –OH and –COOH). Time points were analyzed separately, since vehicle instillation may induce slight inflammation on day 1 (Jacobsen et al., 2009). All MWCNT induced time- and dose-dependently increased neutrophil counts (Figure 2), and numbers correlated with the total number of BAL cells (data not shown).

Day 1

All MWCNT induced a dose-dependent neutrophil influx on day 1. No significant effects were observed for the pristine MWCNT from Group I (NRCWE-040) and all MWCNT from Group II (NRCWE-043 to -045) at dose 6 μg/mouse (Figure 2A), whereas this dose reached significance for all other MWCNT. Group III had significantly more neutrophils, and was thus more inflammogenic, than Group I and II. Within Group I, the pristine NRCWE-040 induced more inflammation than the hydroxylated NRCWE-41.

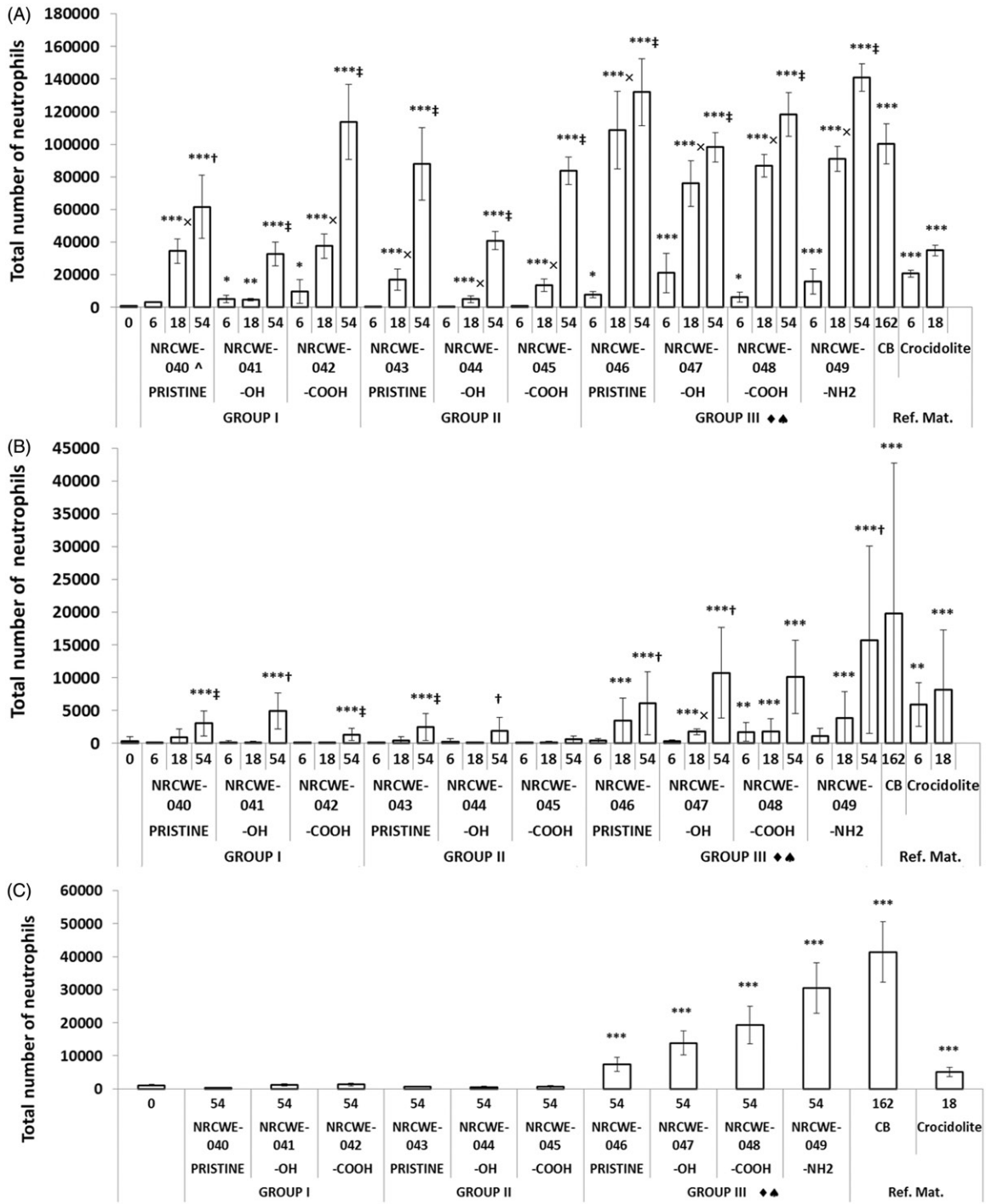

Figure 2. Total number of neutrophils in the BAL fluid after exposure to MWCNT and reference materials. Error bars indicate SD. (A) Day 1. (B) Day 28. (C) Day 92. *$p<0.05$, **$p<0.01$, ***$p<0.001$ compared to vehicle controls. †: 54 > 6 μg/ml; ‡: 54 > 6 and 18 μg/ml; x: 18 > 6 μg/ml; ^: higher than the –OH form; ♦: higher than Group I; ♠: higher than Group II; ♣: higher than Group III.

Day 28

MWCNT-induced inflammation subsided over time (Figure 2B). However, for most doses of MWCNT in Group III, there was still significant neutrophil influx. Also, after instillation of 54 μg/mouse, all MWCNT in Group I and pristine NRCWE-043 in Group II induced significantly increased neutrophils influx.

Day 92

Group III MWCNT (NRCWE-046 to -049) were still inflammogenic on day 92, whereas neutrophil counts in Group I and II had returned to control levels (Figure 2C).

Reference materials

Printex 90 and crocidolite were inflammogenic at all instilled doses and at all time points (Figure 2).

Correlations with instilled surface area and functionalization

The neutrophil counts on day 1 correlated significantly with the total instilled surface area (Figure 3A; $p < 0.0001$). This was also true when doses 6, 18 and 54 μg/mouse were analyzed separately (Figure 3B–D; 6 μg/mouse, $p = 0.01$; 18 μg/mouse, $p < 0.001$; and 54 μg/mouse, $p = 0.056$). The correlation persisted 28 days post-exposure ($p < 0.0001$; for all doses), but only marginally 92 days post-exposure ($p > 0.05$; for all doses) (Supplementary Figure 6). Neutrophil counts were not correlated with functionalization (data not shown).

Correlations with metal contaminants and endotoxin

On day 1, total neutrophil counts correlated with the instilled amounts of Mn, Mg and Co (all $p < 0.0001$, data not shown). These correlations persisted 92 days post-exposure, but the association was weaker on day 28. The total instilled amounts of Ni, Fe and Al did not correlate with the neutrophil counts in the BAL fluid. Endotoxin content did not correlate with neutrophil influx (data not shown).

Multiple regression analysis

Physicochemical parameters (BET surface area, Fe, Mn, Ni, Co, Mg, diameter, length and oxygen content) were analyzed for pairwise associations in a Pearson's correlation analysis: A cluster of parameters (BET surface area, diameter, Mn, Co, Mg and Ni) were highly correlated (Table 2). Log-transformed, BET surface area was chosen as proxy variable for this cluster in the multiple regression analyses.

Of the remaining variables (BET surface area, length, OH and Fe), BET surface area and dose significantly predicted inflammation on all post-exposure days (Table 3). On day 28, length additionally predicted inflammation, whereas oxygen content was protective (Table 3). On day 92, Fe content was protective (Table 3). Multiple regression analyses using log-transformed diameter as proxy variable for the highly correlated cluster are presented in Supplementary Table 4.

Total protein in bronchoalveolar lavage fluid

Instillation of MWCNT induced dose and time-dependent increases in BAL protein in the exposed mice (Supplementary Figure 7). Protein concentration and neutrophil counts in BAL correlated significantly ($p < 0.0001$, $p < 0.0001$ and $p = 0.022$ for 1, 28 and 92 days post-exposure, respectively) (Supplementary Figure 8). The reference material crocidolite induced significantly increased protein content at both instilled doses up to 28 days after exposure. Similar to previous reports (Kyjovska et al., 2015), we observed increased protein content at all-time points after Printex 90 exposure.

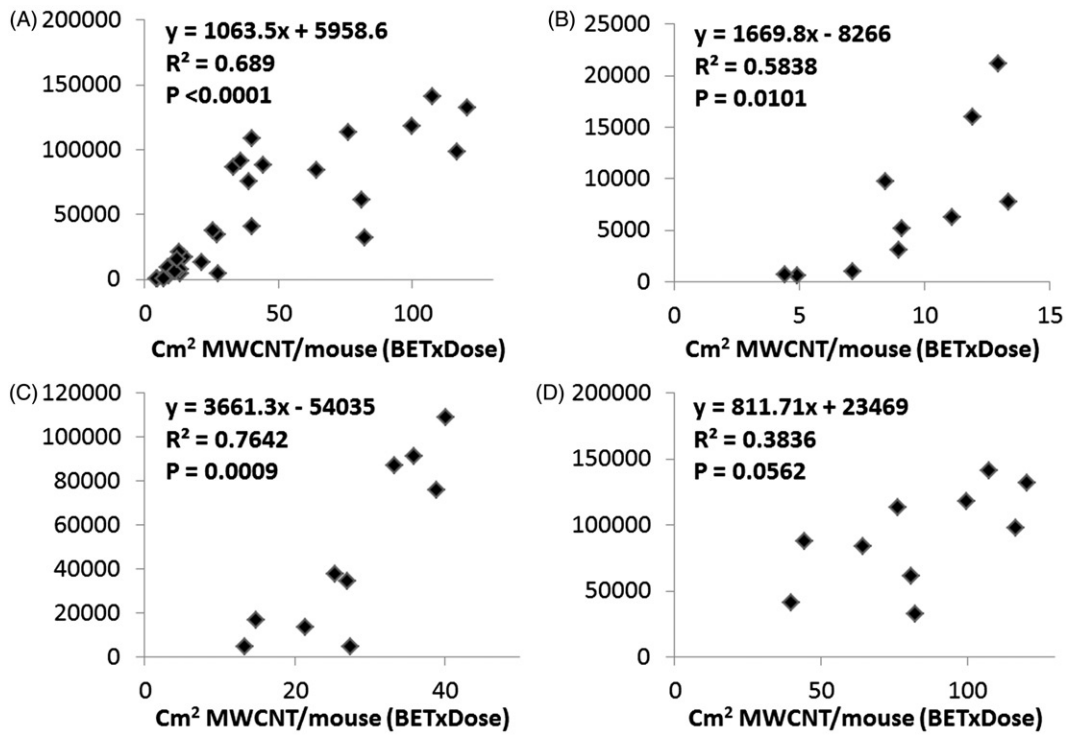

Figure 3. The relationship between total number of neutrophils in the BAL fluid and the total instilled surface area on day 1. Individual data points are the average total neutrophil numbers for each exposure group. The linear relationship, the R^2 and the p value for the correlation are shown for all correlations. (A) All MWCNT types and doses. (B) All MWCNT types at dose 6 μg/mouse. (C) All MWCNT types at dose 18 μg/mouse. (D) All MWCNT types at dose 54 μg/mouse.

DOI: 10.1080/17435390.2016.1202351

Table 3. Multiple regression analyses of MWCNT physicochemical properties as predictors of neutrophil influx and DNA damage.

Neutrophil influx						DNA damage					
In bronchoalveolar lavage						In bronchoalveolar lavage					
Day	Exposure variable	Multiplicative effect	LowerCL	UpperCL	Probt	Day	Exposure variable	Multiplicative effect	LowerCL	UpperCL	Probt
1	**Per doubling in dose**	**2.763**	**2.286**	**3.199**	**<0.0001**	1	Per doubling in dose	1.013	0.988	1.037	0.307
	Per doubling in Fe_2O_3	0.927	0.858	1.002	0.0562		Per doubling in Fe_2O_3	1.006	0.994	1.019	0.309
	Per doubling in OH	0.869	0.718	1.053	0.151		Per doubling in OH	1.028	0.998	1.060	0.069
	Per doubling in length	1.164	0.776	1.746	0.462		Per doubling in length	1.051	0.989	1.117	0.108
	Per 25% difference in BET	**1.212**	**1.070**	**1.373**	**0.003**		**Per 25% difference in BET**	**0.884**	**0.864**	**0.904**	**<.0001**
28	**Per doubling in dose**	**4.342**	**3.360**	**5.611**	**<0.0001**	In lung tissue					
	Per doubling in Fe_2O_3	0.951	0.832	1.086	0.457						
	Per doubling in OH	**0.394**	**0.278**	**0.558**	**<0.0001**	1	Per doubling in dose	0.999	0.965	1.034	0.948
	Per doubling in length	**3.537**	**1.782**	**7.020**	**0.0003**		Per doubling in Fe_2O_3	0.999	0.982	1.018	0.999
	Per 25% difference in BET	**1.908**	**1.528**	**2.383**	**<0.0001**		Per doubling in OH	1.057	1.010	1.106	0.016
92	**Per doubling in Fe_2O_3**	**0.657**	**0.503**	**0.858**	**0.003**		**Per doubling in length**	**0.870**	**0.792**	**0.954**	**0.003**
	Per doubling in OH	1.214	0.650	2.266	0.538		**Per 25% difference in BET**	**0.910**	**0.884**	**0.937**	**<.0001**
	Per doubling in length	2.176	0.603	7.850	0.230	28	Per doubling in dose	1.022	0.989	1.056	0.196
	Per 25% difference in BET	**3.053**	**1.942**	**4.800**	**<0.0001**		Per doubling in Fe_2O_3	1.009	0.992	1.026	0.324
							Per doubling in OH	1.052	1.008	1.097	0.020
							Per doubling in length	1.094	1.003	1.193	0.044
							Per 25% difference in BET	**0.962**	**0.935**	**0.989**	**0.006**

Left: Physicochemical parameters and their influence on neutrophil influx in BAL after intratracheal exposure to MWCNT in a multiple regression analysis. Right: Physicochemical parameters and their influence on DNA damage in BAL and lung tissue after intratracheal exposure to MWCNT in a multiple regression analysis. Significant p values ($p \leq 0.01$) are highlighted in bold.

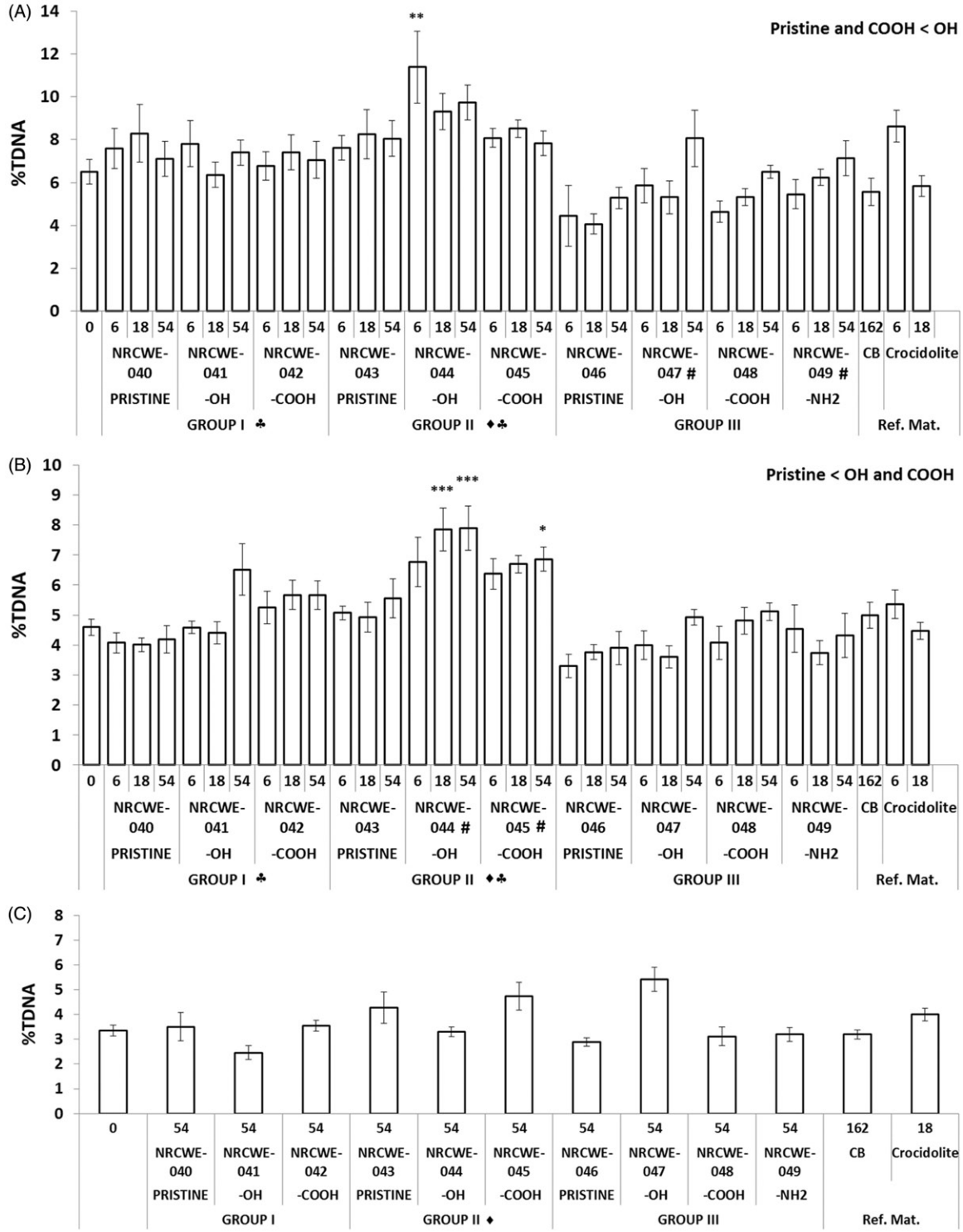

Figure 4. DNA strand breaks in the lung tissue after exposure to MWCNT and reference materials. Error bars indicate SD. (A) Day 1. (B) Day 28. (C) Day 92. *$p < 0.05$, ***$p < 0.001$ compared to vehicle controls. #: higher than the pristine form; ♦: higher than Group I; ♣: higher than Group III.

Analysis of genotoxicity by comet assay

DNA strand breaks in BAL, lung and liver cells on day 1, 28 and 92 days were determined by the comet assay.

BAL

After 1 day, there were significantly more DNA strand breaks for all MWCNT in Group II, except for the dose 54 μg/mouse of the carboxylated MWCNT (NRCWE-045), compared to controls (Supplementary Figure 9). For Group I, all doses of the carboxylated NRCWE-042, the high dose of the pristine NRCWE-040, and the dose 6 μg/mouse of the hydroxylated NRCWE-041 induced DNA damage. No effects were observed for Group III or the reference materials. The effects were significantly greater for Group II than the other groups and were greater in I than III. No changes were observed after 28 and 92 days.

Lung

Except for the dose for the 6 μg/mouse hydroxylated NRCWE-044 in Group II, no significant differences were observed after 1 day (Figure 4A). After 28 days, the level of DNA strand breaks was increased by the two highest doses of hydroxylated NRCWE-

044 and the 54 μg/mouse dose carboxylated NRCWE-045 in Group II compared to controls (Figure 4B). Group II MWCNT induced more DNA strand breaks compared to Group I and III at day 1 and 28. Within Group II, the hydroxylated NRCWE-044 and carboxylated NRCWE-045 induced more DNA strand breaks than the pristine NRCWE-043. No changes were detected at day 92.

Liver

On day 1, only the reference material Printex 90 induced significantly more DNA strand breaks (Supplementary Figure 10).

Exploratory analyses of pairwise associations between DNA strand breaks and physicochemical properties

There were no effects of deposited surface area, metal content, endotoxin content or functionalization on DNA damage except for day 28, where Ni was negatively correlated with DNA damage ($p = 0.03$) and day 92, where deposited surface area (BET × Dose) correlated positively with lung tissue DNA strand break levels ($p = 0.009$) (data not shown). DNA strand breaks correlated positively with diameter size in the lung tissue on day 1 and 28 ($p < 0.0001$ for both time points, Supplementary Figure 11).

Multiple regression analysis

Physicochemical parameters were related to DNA strand breaks in BAL cells and lung tissue by multiple regression analyses. No DNA strand breaks were observed in BAL cells on day 28 and 92, and these time points were therefore not analyzed for this endpoint. An analysis with the remaining variables (BET surface area, length, OH and Fe) showed that BET surface area was significantly protective towards genotoxicity in the BAL cells at day 1, whereas dose had no effect (Table 3).

The levels of DNA strand breaks in lung tissue after MWCNT exposure were only significantly different from control levels on days 1 and 28. Day 92 was therefore excluded from further analyses. A multiple regression analysis with the remaining variables (BET surface area, length, OH and Fe) showed that BET surface area was significantly protective towards DNA strand breaks in lung tissue at day 1 and 28. Length was also protective at day 28 (Table 3), whereas dose had no effect on any tested day. Multiple regression analyses using log-transformed diameter as proxy variable for the highly correlated cluster are presented in Supplementary Table 4 for genotoxicity in BAL cells and lung tissue.

Lung histopathological analysis

Observed histopathological changes on day 28 and 92 are presented in Supplementary Tables 2 and 5–9. The histological changes include lymphocytic aggregates (Lycy), granulomas, occurrence of materials both free and in alveolar macrophages, alveolar macrophage infiltrates, increased thickness of the alveolar duct walls and nearby alveolar septa and focal alveolitis (See grading in Supplementary Table 10). Representative images of the most predominant histological changes are presented in Figure 1. Overall, no clear histopathological differences were observed between the different MWCNT, between groups or across surface functionalizations. However, time and dose dependent differences were observed. No fibrosis was observed at any time point after any MWCNT dose administrated.

Lymphocytic aggregates

The most noticeable finding was Lycy in the lungs of mice exposed to all MWCNT (Supplementary Table 5A and B and Figure 1D–F). Some of these were small (but distinctly larger than in control mice (Figure 1A)) and some were very large, especially in mice exposed to highest doses. Many Lycy were located near the larger vessels, whereas others were located in the vicinity of small bronchi. When Lycy were counted irrespectively of size, scores were slightly higher on post-exposure day 92, especially for the left lung. Lycy scores increased in a dose-dependent manner for all tested materials (Supplementary Table 5A and B). Time-related differences in score were observed for all MWCNT exposures. Progression of Lycy from day 28 to day 92 was observed for all MWCNT exposures, except for NRCWE-40, NRCWE-42 and NRCWE-45, for which regression of Lycy was observed (Supplementary Table 5A). Foreign material or material-laden cells were not detected in the lymphocytic aggregates.

Additional histopathological alterations

Only few multinucleated cell foreign body granulomas were observed overall, and they were mainly seen at the highest dose (Supplementary Table 6 and Figure 1D). Alveolar macrophage infiltrates were scarce in all exposure groups (Supplementary Table 7). A very slight dose-dependent increase in alveolar duct walls and septa thickness in the centriacinar areas was observed for essentially all MWCNT-exposed mice (Supplementary Table 8). Although discrete, this increase was more evident on day 28 than on day 92. The increase was mainly due to mobilization of alveolar type II cells (hyperplasia and hypertrophia) (Figure 1C). Minor focal alveolitis, seen as areas containing small foci with alveolar granular protein-like materials, intact mononuclear cells and alveolar type II cells, was observed in 7 of the 54 μg/mouse exposure groups on 28 days and correspondingly only in 2 groups on day 90 (Figure 1F and Supplementary Table 9).

Control samples

Pulmonary fibrosis was not observed after crocidolite exposure. Few animals in this group displayed slight increase in epithelial cellularity of bronchiolar walls in some areas, but across the whole crocidolite group, the lungs remained essentially without histopathological findings. Pulmonary parenchyma displayed no abnormal finding in the negative control group.

Discussion

We investigated biological effects of a matrix of ten MWCNT subdivided into three groups by length/diameter, and across different surface functionalizations (pristine, OH–, COOH– and one with an amino-function) with the aim to identify potential physicochemical drivers of MWCNT-induced inflammation and genotoxicity. The MWCNT were well-characterized in regards to their key physicochemical characteristics, both in their pristine form and in the vehicle. The MWCNT varied both across groups and within groups in metal content, BET surface area, thickness, length and level of functionalization (Table 1). Overall, the studied MWCNT were relatively short, and greater similarities were observed within groups compared to between groups. Endotoxin content was detectable on almost all MWCNT (Table 1), with the highest level observed for NRCWE-046 (0.34 EU/mg). Endotoxin content did not correlate with neutrophil influx or DNA damage. In addition, the highest endotoxin concentration administrated (0.91 EU/kg body weight for mice at 20 g) was considerably below the endotoxin tolerance limit for human and veterinary drugs (5 EU/kg body weight/h) (USP 30 NF 25 2007). The detected endotoxin content was therefore considered negligible.

Female C57BL/6J mice were exposed by intratracheal instillation at doses 0, 6, 18 or 54 μg MWCNT/mouse and

killed on day 1, 28 or 92. Intratracheal instillation offers precise, safe, cost-effective dosing with a fairly even distribution in the lung (Mikkelsen et al., 2011) and was used to ensure similar dose levels for the different MWCNT. The doses were within the dose range of other instillation/aspiration studies (Kim et al., 2014; Porter et al., 2010; Snyder-Talkington et al., 2013), and they correspond to a third, 1 or 3 times the expected 40-year exposure for workers at the recommended exposure limit of 1 μg carbon/m^3 (NIOSH, 2013), when assuming 10% deposition (Ma-Hock et al., 2009), a ventilation rate of 1.8 l/h for mice, and a 40 h working week. However, higher occupational CNT exposure concentrations of 30-300 μg/m^3 have been reported (Birch et al., 2011; Han et al., 2008; Lee et al., 2010). Furthermore, repeated exposure to CNT may result in accumulation in the lungs over time due to their high bio-persistence (Elgrabli et al., 2008). The doses are therefore relevant. Printex 90 and crocidolite were included for comparison with previous studies (Bourdon et al., 2012b; Jacobsen et al., 2009; Poulsen et al., 2013, 2015a,b). MWCNT were generally shorter than reported by the manufacturer. It is possible that some shortening may have occurred during sonication. The instilled MWCNT appeared well distributed in the lungs on day 28, and MWCNT were still present on day 92 (Figure 1 and Supplementary Table 2). As expected, there were predominantly more foreign material-containing macrophages (Supplementary Table 2) and Lycy-positive cells (Supplementary Table 6A and B) in the left lung, compared to the right lung. This is because the bifurcation to the left lung lobe is positioned slightly elevated to the right lung bifurcation. However, Lycy and foreign material-containing macrophages were widespread in most of the lobes of the right lung, indicating successful instillations. The positive control, Printex 90, induced significant neutrophil influx at all time points (Figure 2), and increased levels of DNA strand breaks in the liver tissue on day 1 (Supplementary Figure 10), in overall agreement with previous reports (Bourdon et al., 2012b; Husain et al., 2015; Jacobsen et al., 2009; Kyjovska et al., 2015).

Influx of inflammatory cells (especially neutrophils) determined by BAL cell composition is a cardinal indicator of lung inflammation. BET surface area of the MWCNT correlated strongly with neutrophil influx in BAL at all assessed days, even after adjustment for the other variables, and after stratification by dose (Figure 3 and Table 3). This indicates that a larger BET surface area of MWCNT results in more neutrophil influx. This is in concordance with previous studies reporting that total deposited surface area of spherical nanomaterials predicts inflammation (Donaldson & Stone, 2003; Duffin et al., 2007; Nakanishi et al., 2015; Sager & Castranova, 2009).

We observed a strong covariation between BET surface area, MWCNT diameter, Mn, Mg and Co content (Table 2) and we were unable to separate these variables in the multiple regression analyses. BET surface area is inherently inversely correlated to diameter. The thin Group III MWCNT contained more than a 100-fold more Mn than the other groups. BET surface area and diameter therefore correlated strongly with Mn. Mn has been related to adverse health effects (reviewed in (Bowman et al., 2011; Crossgrove & Zheng, 2004), but it is also an essential element. Considering the required intake, it is therefore unlikely that the present low amounts drive toxicity. Mg was included in the cluster of highly correlated parameters. However, since the concentrations of Mg identified in the present study are unlikely to be toxic (Kuschner et al., 1997), Mg was not considered a plausible determinant of inflammation. Ni showed strong positive correlation with diameter and negative correlation with BET surface area, Mn, Mg and Co, as only the thicker MWCNT (Group II) contained Ni. Ni compounds are toxic and considered human carcinogens (IARC Working Group on the Evaluation of Carcinogenic Risks to Humans, 2012). The seemingly protective effect of Ni on inflammation is therefore likely driven by covariance with the other cluster parameters. Co correlated positively with BET surface area, Mn and Mg, and negatively with diameter and Ni. Excessive pulmonary exposure to Co has been reported to result in adverse pulmonary effects (NIOSH, 1978), and Co has been classified as possibly carcinogenic to humans (IARC Working Group on the Evaluation of Carcinogenic Risks to Humans, 2006). Cobalt is therefore a possible predictor of inflammation. However, based on the overall analyses (correlations and multiple regression) and previous literature, we suggest that the deposited surface area of MWCNT is the primary determinant of the neutrophil influx after pulmonary MWCNT exposure.

The MWCNT induced group dependent lung genotoxicity in BAL fluid and lung tissue. In the adjusted analyses, BET surface area was significantly protective against DNA damage in both BAL fluid and lung tissue (Table 3). This is most likely because BET surface area correlates strongly and inversely with diameter. Indeed, larger diameter was a significant predictor of genotoxicity in both BAL cells and lung tissue (Supplementary Table 4). Thus, thicker MWCNT with small surface area were more genotoxic than thinner MWCNT with larger surface area. Diameter predicted DNA damage independently of length (no correlation between length and diameter) and dose. Interestingly, diameter and DNA damage were also related in our previous *in vitro* investigation using the same MWCNT (Jackson et al., 2015).

Length has been proposed as a driver of MWCNT-induced toxicity (Donaldson et al., 2010; Murphy et al., 2011; Poland et al., 2008). Long MWCNT conform to the fiber paradigm, and may cause frustrated phagocytosis. However, the proposed threshold of the CNT length for frustrated phagocytosis is 10–20 μm. All the MWCNT used in the present study were shorter (Table 1), and surprisingly, the average lengths of the groups did not vary much. It is possible that the MWCNT were shortened during sonication, which was used to disperse the MWCNT. The distributions of the MWCNT lengths were highly skewed in this study as indicated by the large standard deviations. The hydroxylated MWCNT in Group I, all in Group II, and the pristine, carboxylated and aminated MWCNT in Group III all included a substantial proportion of tubes longer than 5 μm (Supplementary Figure 5). MWCNT of intermediate lengths (3–10 μm) have been reported to induce intracellular stress and to escape from vesicle enclosures in macrophages (Kobler et al., 2015), which could explain the length-dependent inflammation observed on day 28 in the present study (Table 3). However, because of the narrow range of lengths we were not able to detect effects of length on neutrophil influx at day 1 and 92. We observed a protective effect of length on lung genotoxicity on day 1. In agreement with this, crocidolite induced neutrophil influx in BAL fluid and no genotoxicity, despite being long and rigid (Figures 2 and 4 and Supplementary Figures 9 and 10). This indicates that properties other than length are more important for genotoxicity.

In contrast to our previous observations (Poulsen et al., 2015b), we observed no collagen-stained areas, indicative of pulmonary fibrosis after MWCNT exposure. We have previously reported fibrogenicity of another MWCNT, that was thicker and consistently longer (Poulsen et al., 2015b). As reported in the literature, long, fiber-like CNT are more fibrogenic than curved entangled CNT (Murphy et al., 2011; Poland et al., 2008).

Oxygen content of MWCNT (–OH and –COOH) did not covariate with other properties and was identified as protective of

inflammation on day 28 in the multiple regression analysis (Tables 2–3). Lower or elimination of cytotoxicity has previously been reported in *in vitro* studies of carboxylated CNT (Hamilton et al., 2013; Sayes et al., 2006). Similarly, carboxylated MWCNT were less toxic than pristine ones after i.v. injection or pharyngeal aspiration (Jain et al., 2011; Sager et al., 2014). Higher surface density of oxidized groups on the MWCNT may increase their hydrophilicity and dispersion in the lung. Structural defects may also be induced during the chemical treatment. This renders the MWCNT more susceptible for enzymatic and oxidative breakage, resulting in greater bio-degradability and thus more effective clearance from the lungs (Liu et al., 2010). This may explain the possibly protective effect of oxygen content on inflammation seen in the present study. However, further studies using a larger array of MWCNT are required to discern this.

The most noticeable histopathological change was the increased number of lymphocytic aggregates (Lycy) in the lung tissue on day 28 and 92 (Figure 1(D–F) and Supplementary Table 5A and B). To our knowledge, this is the first time Lycy have been described in association with nanomaterials. The severity was dose- and time-dependent, but there were no clear differences between groups or functionalization. Similarly, dose-dependent lymphocytic influx in the BAL fluid was observed for all MWCNT exposures (except NRCWE-045) on day 28 (Supplementary Table 3). This had resolved on day 92. We have previously reported lymphocytic influx in BAL fluid and lymphoid cell infiltration in the lung tissue of mice 28 days after exposure to MWCNT of very different physicochemical properties (Poulsen et al., 2015b). This indicates that exposure to MWCNT, regardless of physicochemical properties, induces influx of lymphocytes into the BAL fluid, which results in subsequent increased Lycy in the lung tissue, leading to chronic lymphocytic inflammation. Predominant pulmonary TH2 infiltration, together with a large neutrophilic influx in the BAL fluid, has also been reported after repeated silica-coated TiO_2 inhalation exposures in female BALB/c mice (Leppanen et al., 2015). In the present study, this was observed already after a single instillation of MWCNT. For Printex 90, this was observed only at higher doses (Bourdon et al., 2012b; Kyjovska et al., 2015).

In most reports on MWCNT toxicity, only one or two MWCNT were studied. Using a panel of 10 MWCNT, we attempted to identify specific physicochemical drivers of MWCNT-induced pulmonary inflammation and genotoxicity in a known mouse model. With this hypothesis-generating approach, we identified BET surface area, or diameter, as a predictor of pulmonary inflammation and genotoxicity. However, even though the panel of MWCNT is large in a nanotoxicology context, the dataset is still small from a statistical point-of-view. One limitation is the large covariance between parameters. Ideally, we would test the hypotheses generated in this study, using a larger array of MWCNT. This would allow determination of toxicity-inducing physicochemical characteristics and thus safe-by-design CNT.

A recent study on pulmonary exposure to two unrelated MWCNT showed that a short, thin, entangled type of MWCNT induced more pulmonary inflammation than a longer and thicker fiber-like MWCNT type (Poulsen et al., 2015b). Only the longer and thicker MWCNT induced fibrosis. This supports the hypotheses generated in this study and at the same time highlights the difficulty in generating safe MWCNT. Thick and long MWCNT have increased fibrotic and genotoxic potential, whereas thin and short MWCNT induce stronger and more long-lasting inflammation, which may lead to increased risk of cardiovascular disease through a long-lasting acute phase response (Poulsen et al., 2015a). Either effect is undesirable. Studies analyzing many MWCNT are needed to bring us closer to safe-by-design MWCNT.

Conclusion

The 10 studied MWCNT induced dose-, time- and MWCNT-dependent neutrophil influx in BAL and DNA damage in the C57BL/6J mice. BET surface area was a positive predictor of inflammation, measured as neutrophil influx in BAL fluid, on all post-exposure days. MWCNT diameter size, and thus BET surface area, significantly predicted genotoxicity in BAL fluid and lung tissue, such that small BET surface area and hence large MWCNT diameter was associated with increased genotoxicity. Oxidation of MWCNT was protective for inflammation on day 28, whereas length was a predictor. This study provides information on possible toxicity-driving physicochemical properties of MWCNT, which in turn can be used for safe-by-design manufacturing of MWCNT.

Acknowledgements

Technical assistance from Michael Guldbrandsen, Eva Terrida, Lourdes Pedersen, Elzbieta Christiansen, Inge Christiansen, Ulla Tegner, Anne Abildtrup, Yahia Kembouche, Anne-Karin Asp is greatly appreciated. Especially thanks to Kathrine Bjørneboe from the Danish Technological Institute for producing the SEM images of MWCNT and reference material in instillation dilutions.

Declaration of interest

The authors report no conflicts of interest. The project was supported by Danish Center for Nanosafety, grant # 20110092173-3 from the Danish Working Environment Research Foundation and the European Union Seventh Framework Program [FP7/2007–2013] under grant agreement # 310584 [NANoREG].

References

Birch ME, Ku BK, Evans DE, Ruda-Eberenz TA. 2011. Exposure and emissions monitoring during carbon nanofiber production–Part I: elemental carbon and iron-soot aerosols. Ann Occup Hyg 55:1016–36.

Borm PJ, Driscoll K. 1996. Particles, inflammation and respiratory tract carcinogenesis. Toxicol Lett 88:109–13.

Bourdon JA, Halappanavar S, Saber AT, Jacobsen NR, Williams A, Wallin H, et al. 2012a. Hepatic and pulmonary toxicogenomic profiles in mice intratracheally instilled with carbon black nanoparticles reveal pulmonary inflammation, acute phase response, and alterations in lipid homeostasis. Toxicol Sci 127:474–84.

Bourdon JA, Saber AT, Jacobsen NR, Jensen KA, Madsen AM, Lamson JS, et al. 2012b. Carbon black nanoparticle instillation induces sustained inflammation and genotoxicity in mouse lung and liver. Part Fibre Toxicol 9:5.

Bowman AB, Kwakye GF, Herrero HE, Aschner M. 2011. Role of manganese in neurodegenerative diseases. J Trace Elem Med Biol 25: 191–203.

Cooke MS, Evans MD, Dizdaroglu M, Lunec J. 2003. Oxidative DNA damage: mechanisms, mutation, and disease. FASEB J 17:1195–214.

Crossgrove J, Zheng W. 2004. Manganese toxicity upon overexposure. NMR Biomed 17:544–53.

Donaldson K, Murphy FA, Duffin R, Poland CA. 2010. Asbestos, carbon nanotubes and the pleural mesothelium: a review of the hypothesis regarding the role of long fibre retention in the parietal pleura, inflammation and mesothelioma. Part Fibre Toxicol 7:5.

Donaldson K, Stone V. 2003. Current hypotheses on the mechanisms of toxicity of ultrafine particles. Ann Ist Super Sanita 39:405–10.

Duffin R, Tran L, Brown D, Stone V, Donaldson K. 2007. Proinflammogenic effects of low-toxicity and metal nanoparticles *in vivo* and *in vitro*: highlighting the role of particle surface area and surface reactivity. Inhal Toxicol 19:849–56.

Elgrabli D, Floriani M, bella-Gallart S, Meunier L, Gamez C, Delalain P, et al. 2008. Biodistribution and clearance of instilled carbon nanotubes in rat lung. Part Fibre Toxicol 5:20.

Erdely A, Hulderman T, Salmen R, Liston A, Zeidler-Erdely PC, Schwegler-Berry D, et al. 2009. Cross-talk between lung and systemic

circulation during carbon nanotube respiratory exposure. Potential biomarkers. Nano Lett 9:36–43.

Federico A, Morgillo F, Tuccillo C, Ciardiello F, Loguercio C. 2007. Chronic inflammation and oxidative stress in human carcinogenesis. Int J Cancer 121:2381–6.

Grosse Y, Loomis D, Guyton KZ, Lauby-Secretan B, Ghissassi FE, Bouvard V, et al. 2014. Carcinogenicity of fluoro-edenite, silicon carbide fibres and whiskers, and carbon nanotubes. The Lancet Oncol 15:1427–8.

Hamilton Jr. RF,, Wu Z, Mitra S, Shaw PK, Holian A. 2013. Effect of MWCNT size, carboxylation, and purification on *in vitro* and *in vivo* toxicity, inflammation and lung pathology. Part Fibre Toxicol 10:57.

Han JH, Lee EJ, Lee JH, So KP, Lee YH, Bae GN, et al. 2008. Monitoring multiwalled carbon nanotube exposure in carbon nanotube research facility. Inhal Toxicol 20:741–9.

Husain M, Kyjovska ZO, Bourdon-Lacombe J, Saber AT, Jensen KA, Jacobsen NR, et al. 2015. Carbon black nanoparticles induce biphasic gene expression changes associated with inflammatory responses in the lungs of C57BL/6 mice following a single intratracheal instillation. Toxicol Appl Pharmacol 289:573–88.

Husain M, Saber AT, Guo C, Jacobsen NR, Jensen KA, Yauk CL, et al. 2013. Pulmonary instillation of low doses of titanium dioxide nanoparticles in mice leads to particle retention and gene expression changes in the absence of inflammation. Toxicol Appl Pharmacol 269: 250–62.

IARC Working Group on the Evaluation of Carcinogenic Risks to Humans. 2006. Cobalt in hard metals and cobalt sulfate, gallium arsenide, indium phosphide and vanadium pentoxide. IARC Monogr Eval Carcinog Risks Hum 86:1–294.

IARC Working Group on the Evaluation of Carcinogenic Risks to Humans. 2012. Nickel and nickel compounds. IARC Monogr 100C: 169–218.

Jackson P, Hougaard KS, Vogel U, Wu D, Casavant L, Williams A, et al. 2011. Exposure of pregnant mice to carbon black by intratracheal instillation: toxicogenomic effects in dams and offspring. Mutat Res 745:73–83.

Jackson P, Kling K, Jensen KA, Clausen PA, Madsen AM, Wallin H, Vogel U. 2015. Characterization of genotoxic response to 15 multi-walled carbon nanotubes with variable physicochemical properties including surface functionalizations in the FE1-Muta(TM) mouse lung epithelial cell line. Environ Mol Mutagen 56:183–203.

Jacobsen NR, Moller P, Jensen KA, Vogel U, Ladefoged O, Loft S, Wallin H. 2009. Lung inflammation and genotoxicity following pulmonary exposure to nanoparticles in ApoE-/- mice. Part Fibre Toxicol 6:2.

Jacobsen NR, Pojana G, White P, Moller P, Cohn CA, Korsholm KS, et al. 2008. Genotoxicity, cytotoxicity, and reactive oxygen species induced by single-walled carbon nanotubes and C(60) fullerenes in the FE1-Mutatrade markMouse lung epithelial cells. Environ Mol Mutagen 49:476–87.

Jacobsen NR, Saber AT, White P, Moller P, Pojana G, Vogel U, et al. 2007. Increased mutant frequency by carbon black, but not quartz, in the lacZ and cII transgenes of muta mouse lung epithelial cells. Environ Mol Mutagen 48:451–61.

Jain S, Thakare VS, Das M, Godugu C, Jain AK, Mathur R, et al. 2011. Toxicity of multiwalled carbon nanotubes with end defects critically depends on their functionalization density. Chem Res Toxicol 24: 2028–39.

Kim JE, Lee S, Lee AY, Seo HW, Chae C, Cho MH. 2014. Intratracheal exposure to multi-walled carbon nanotubes induces a nonalcoholic steatohepatitis-like phenotype in C57BL/6J mice. Nanotoxicology 9: 13–23.

Kobler C, Poulsen SS, Saber AT, Jacobsen NR, Wallin H, Yauk C, et al. 2015. Time-dependent subcellular distribution and effects of carbon nanotubes in lungs of mice. PLoS One 10:e0116481.

Kuschner WG, Wong H, D'Alessandro A, Quinlan P, Blanc PD. 1997. Human pulmonary responses to experimental inhalation of high concentration fine and ultrafine magnesium oxide particles. Environ Health Perspect 105:1234–7.

Kyjovska ZO, Jacobsen NR, Saber AT, Bengtson S, Jackson P, Wallin H, Vogel U. 2015. DNA damage following pulmonary exposure by instillation to low doses of carbon black (Printex 90) nanoparticles in mice. Environ Mol Mutagen 56:41–9.

Lee JH, Lee SB, Bae GN, Jeon KS, Yoon JU, Ji JH, et al. 2010. Exposure assessment of carbon nanotube manufacturing workplaces. Inhal Toxicol 22:369–81.

Leppanen M, Korpi A, Mikkonen S, Yli-Pirila P, Lehto M, Pylkkanen L, et al. 2015. Inhaled silica-coated TiO_2 nanoparticles induced airway irritation, airflow limitation and inflammation in mice. Nanotoxicology 9:210–18.

Liu X, Hurt RH, Kane AB. 2010. Biodurability of single-walled carbon nanotubes depends on surface functionalization. Carbon NY 48: 1961–9.

Ma-Hock L, Treumann S, Strauss V, Brill S, Luizi F, Mertler M, et al. 2009. Inhalation toxicity of multiwall carbon nanotubes in rats exposed for 3 months. Toxicol Sci 112:468–81.

Mikkelsen L, Sheykhzade M, Jensen KA, Saber AT, Jacobsen NR, Vogel U, et al. 2011. Modest effect on plaque progression and vasodilatory function in atherosclerosis-prone mice exposed to nanosized TiO(2). Part Fibre Toxicol 8:32.

Morimoto Y, Hirohashi M, Ogami A, Oyabu T, Myojo T, Todoroki M, et al. 2012. Pulmonary toxicity of well-dispersed multi-wall carbon nanotubes following inhalation and intratracheal instillation. Nanotoxicology 6:587–99.

Muhle H, Pott F, Bellmann B, Takenaka S, Ziem U. 1987. Inhalation and injection experiments in rats to test the carcinogenicity of MMMF. Ann Occup Hyg 31:755–64.

Murphy FA, Poland CA, Duffin R, Al-Jamal KT, li-Boucetta H, Nunes A, et al. 2011. Length-dependent retention of carbon nanotubes in the pleural space of mice initiates sustained inflammation and progressive fibrosis on the parietal pleura. Am J Pathol 178:2587–600.

Nakanishi J, Morimoto Y, Ogura I, Kobayashi N, Naya M, Ema M, et al. 2015. Risk assessment of the carbon nanotube group. Risk Anal 35: 1940–56.

NIOSH. 1978. Occupational Safety and Health Guideline for Cobalt. Washington: U.S. Department of Health & Human Services, 1–5.

NIOSH. 2013. Current intelligence bulletin 65: Occupational Exposure to Carbon Nanotubes and Nanofibers. DHHS Publication No. 2013–145. Washington: U.S. Department of Health & Human Services, 1–184.

Poland CA, Duffin R, Kinloch I, Maynard A, Wallace WA, Seaton A, et al. 2008. Carbon nanotubes introduced into the abdominal cavity of mice show asbestos-like pathogenicity in a pilot study. Nat Nanotechnol 3:423–8.

Porter DW, Hubbs AF, Mercer RR, Wu N, Wolfarth MG, Sriram K, et al. 2010. Mouse pulmonary dose- and time course-responses induced by exposure to multi-walled carbon nanotubes. Toxicology 269:136–47.

Poulsen SS, Jacobsen NR, Labib S, Wu D, Husain M, Williams A, et al. 2013. Transcriptomic analysis reveals novel mechanistic insight into murine biological responses to multi-walled carbon nanotubes in lungs and cultured lung epithelial cells. PLoS One 8:e80452.

Poulsen SS, Saber AT, Mortensen A, Szarek J, Wu D, Williams A, et al. 2015a. Changes in cholesterol homeostasis and acute phase response link pulmonary exposure to multi-walled carbon nanotubes to risk of cardiovascular disease. Toxicol Appl Pharmacol 283:210–22.

Poulsen SS, Saber AT, Williams A, Andersen O, Kobler C, Atluri R, et al. 2015b. MWCNTs of different physicochemical properties cause similar inflammatory responses, but differences in transcriptional and histological markers of fibrosis in mouse lungs. Toxicol Appl Pharmacol 284:16–32.

Rittinghausen S, Hackbarth A, Creutzenberg O, Ernst H, Heinrich U, Leonhardt A, Schaudien D. 2014. The carcinogenic effect of various multi-walled carbon nanotubes (MWCNTs) after intraperitoneal injection in rats. Part Fibre Toxicol 11:59.

Saber AT, Jacobsen NR, Jackson P, Poulsen SS, Kyjovska ZO, Halappanavar S, et al. 2014. Particle-induced pulmonary acute phase response may be the causal link between particle inhalation and cardiovascular disease. Wiley Interdiscip Rev Nanomed Nanobiotechnol 6:517–31.

Saber AT, Lamson JS, Jacobsen NR, Ravn-Haren G, Hougaard KS, Nyendi AN, et al. 2013. Particle-induced pulmonary acute phase response correlates with neutrophil influx linking inhaled particles and cardiovascular risk. PLoS One 8:e69020.

Sager TM, Castranova V. 2009. Surface area of particle administered versus mass in determining the pulmonary toxicity of ultrafine and fine carbon black: comparison to ultrafine titanium dioxide. Part Fibre Toxicol 6:15.

Sager TM, Wolfarth MW, Andrew M, Hubbs A, Friend S, Chen TH, et al. 2014. Effect of multi-walled carbon nanotube surface modification on bioactivity in the C57BL/6 mouse model. Nanotoxicology 8: 317–27.

Sayes CM, Liang F, Hudson JL, Mendez J, Guo W, Beach JM, et al. 2006. Functionalization density dependence of single-walled carbon nanotubes cytotoxicity *in vitro*. Toxicol Lett 161:135–42.

Snyder-Talkington BN, Dymacek J, Porter DW, Wolfarth MG, Mercer RR, Pacurari M, et al. 2013. System-based identification of toxicity pathways associated with multi-walled carbon nanotube-induced pathological responses. Toxicol Appl Pharmacol 272: 476–89.

Ursini CL, Cavallo D, Fresegna AM, Ciervo A, Maiello R, Buresti G, et al. 2012. Comparative cyto-genotoxicity assessment of functionalized and pristine multiwalled carbon nanotubes on human lung epithelial cells. Toxicol In Vitro 26:831–40.

USP 30 NF 25. 2007. *Bacterial endotoxins test*.

Valko M, Rhodes CJ, Moncol J, Izakovic M, Mazur M. 2006. Free radicals, metals and antioxidants in oxidative stress-induced cancer. Chem Biol Interact 160:1–40.

Supplementary material available online

Supplementary Tables S1-S10 and Figures S1-S11